

Derivation of the Matalon-Packter law for Liesegang patterns

T. Antal

Institute for Theoretical Physics, Eötvös University, 1088 Budapest, Puskin u. 5-7, Hungary

M. Droz and J. Magnin

Département de Physique Théorique, Université de Genève, CH 1211 Genève 4, Switzerland

Z. Rácz^{a)}

Department of Physics, Theoretical Physics, Oxford University, 1 Keble Road, Oxford OX1 3NP, United Kingdom

M. Zrinyi

Department of Physical Chemistry, Technical University of Budapest, H-1521 Budapest, Hungary

(Received 22 July 1998; accepted 24 August 1998)

Theoretical models of the Liesegang phenomena are studied and simple expressions for the spacing coefficients characterizing the patterns are derived. The emphasis is on displaying the explicit dependences on the concentrations of the inner and the outer electrolytes. Competing theories (ion-product supersaturation, nucleation and droplet growth, induced sol-coagulation) are treated with the aim of finding the distinguishing features of the theories. The predictions are compared with experiments and the results suggest that the induced sol-coagulation theory is the best candidate for describing the experimental observations embodied in the Matalon-Packter law.
© 1998 American Institute of Physics. [S0021-9606(98)50145-6]

I. INTRODUCTION

Systems that exhibit pattern formation are common in nature, and patterns often emerge in the wake of a moving front.¹ A well known example that will be studied below is the Liesegang phenomenon,^{2,3} the formation of precipitation patterns by a moving chemical reaction front. In a typical experimental setup, one has a chemical reactant (inner electrolyte) dissolved in a gel matrix and a second reactant (outer electrolyte) poured onto the gel. The concentration of the outer electrolyte is much higher than that of the inner one and so it diffuses into the gel and reacts with the inner reactant. The reaction product then precipitates and, frequently, the observed precipitation patterns are a family of bands or rings (depending on the geometry of the system) clearly separated in the direction perpendicular to the diffusion. This process is believed to be responsible for many precipitation patterns such as the structure of agate rocks³ or, to cite a somewhat speculative example, the pattern of human gallstones.

Although the Liesegang patterns have been known for more than 100 years,² there is still disagreement as to the mechanisms underlying this phenomenon. The main problem is the lack of a theory that could be compared with experiments quantitatively and, to a lesser degree, the lack of experiments that produce results amenable to quantitative theoretical analysis. At first the task appears to be simple. The Liesegang bands are formed at times t_n at some positions x_n (measured from the planes separating the reagents at the initial moment), and have a width w_n . The quantities t_n , x_n and w_n obey the following generic laws:

(i) After a transient time, the position x_n of the n th band is related to the time t_n of its formation through the so-called *time law*, $x_n \sim \sqrt{t_n}$, first discussed in Ref. 4. The time law is a rather obvious consequence of the diffusive motion of a reaction front in a gel and thus it is considered to be understood.

(ii) For large n , the ratio of the positions of two consecutive bands approaches a constant value

$$\frac{x_n}{x_{n-1}} \rightarrow 1 + p, \quad (1)$$

with $0.05 < p < 0.4$ typically. This last property is known as the Jablczynski law,⁵ or the *spacing law*, and $1 + p$ is called the *spacing coefficient*. Most of the detailed experimental observations concern this law. It has been found that the spacing coefficient is a nonuniversal quantity. It depends, for example, on the concentrations a_0 and b_0 of the outer and inner electrolytes which can be controlled experimentally. Based on several different experiments, Matalon and Packter^{6,7} concluded that

$$p = F(b_0) + \frac{G(b_0)}{a_0}, \quad (2)$$

where F and G are decreasing functions of their arguments. For various reagents, they found $F(b_0) \sim b_0^{-\gamma}$ with $0.2 \leq \gamma \leq 2.7$. The function $G(b_0)$ is less known but it is generally observed that it decreases with increasing b_0 . The observation expressed in Eq. (2) is usually called the *Matalon-Packter law*.

A problem with the Matalon-Packter law is that, experimentally, a_0 and b_0 can usually be changed only by a factor 5-10 and, furthermore, p itself has a significant error bar

^{a)}Permanent address: Institute for Theoretical Physics, Eötvös University, 1088 Budapest, Puskin u.5-7, Hungary.

since it is determined from a finite number of x_n -s ($n \sim 10 - 20$). Thus the functional form (2) is far from unique; it should be considered as a power law fit to p .⁸

(iii) Finally, the *width law* states that the width w_n of the n -th band is an increasing function of n and typically $w_n \sim x_n^\alpha$, $\alpha > 0$.⁹ Since the definition of w_n is open to debate and the error bars in the measurements of w_n are rather large, this quantity has largely been ignored in the quantitative discussions of Liesegang phenomena.

Although there are a large number of interesting and often puzzling observations about Liesegang phenomena in particular systems, the above three points appear to be the only ones which describe quantifiable results and carry some generality.

One would expect that so few experimental facts can be explained easily. Indeed, there are several competing theories,¹⁰⁻²¹ many of which¹⁰⁻¹⁷ fare well as far as the derivation of the time and spacing laws are concerned.²² All these theories follow how the diffusive reagents (ions in the outer and inner electrolytes) A and B turn into immobile precipitate D ,



by taking into account various scenarios for the intermediate steps denoted as $\dots C \dots$. Since the precipitate appears through some kind of supersaturation, further differences in theories arise from the details of treating the nucleation thresholds and the growth kinetics of the precipitate.

The simplest (and first developed) theory is based on the concept of *supersaturation of ion-product*¹⁰ and has been developed by many researchers.^{11-13,23} In this theory, there is no intermediate step in between A, B and D . When the local product of the concentrations of the reactants, ab , reaches some critical value, q^* , nucleation of the precipitate D occurs. The nucleated particles grow and deplete A and B in their surroundings. As a consequence, the local level of ab drops and no new nucleation takes place. This continues until the reaction zone (where ab is maximum) moves far enough that the depletion effect of the precipitate becomes weak. Then $ab = q^*$ is reached again and nucleation can occur. The repetition of this process leads to the formation of bands.

In the next level of complexity, theories contain a single intermediate step in $\dots C \dots$ with the mechanism of band formation based on the supersaturation of the intermediate compound C .^{16,17} It is assumed that A and B react to produce a new species C which also diffuses in the gel. The nature of C is not really specified; it may be a molecule as well as a colloid particle. When the local concentration of C reaches some threshold value, nucleation occurs and the nucleated particles, D , act as aggregation seeds. The C particles near to D aggregate to the existing droplet (hence become D) provided their local concentration is larger than a given aggregation threshold. These models are characterized by two thresholds, one for nucleation and one for droplet growth. The depletion mechanism is similar to the one described for the ion-product theory and it leads to band formation. We shall refer to this theory as the theory of *nucleation and droplet growth*.

A variation of the single intermediate compound theories is based on the idea of an *induced sol-coagulation* process.^{14,15} The compound C is assumed to be the sol and this sol coagulates if the following two conditions are satisfied. First, the concentration of C exceeds a supersaturation threshold $c \geq c^*$ and, second, the local concentration of the outer electrolyte is above a threshold $a > a^*$ that is often referred to as the critical coagulation concentration threshold. The band formation is a consequence of the nucleation and growth of the precipitate combined with the motion of the front where $a = a^*$.

The time- and the spacing laws follow from the above theories. Thus, to select the correct theory (provided there is a single theory for all Liesegang phenomena), one would have to calculate the functional form of $p(a_0, b_0)$ in order to find agreement or disagreement with the Matalon-Packter law. The spacing coefficient, however, is obtained from the numerical solution of complicated coupled nonlinear differential equations and, as a consequence, the results are in an implicit form that is not particularly useful for deducing $p(a_0, b_0)$. A notable exception is the simplest version of the ion-product theory which was used by Wagner¹¹ to derive a result, $p \sim a_0^{-2/3}$, that is at variance with the Matalon-Packter law. Wagner's result raises the question whether the present theories contain the Matalon-Packter law at all and our aim here is to discuss this question and make an attempt at answering it.

In attempting to derive the Matalon-Packter law, our basic aim is to keep the calculations and formulas simple so that the explicit dependence on a_0 and b_0 could be displayed. Accordingly, we have to make simplifying assumptions. The first two of these assumptions are about the experimental setup and the majority of the experiments satisfy the constraints described there. The remaining assumptions are based on observations of the time evolution of the concentrations of the reactants and reaction products obtained from numerical solution of the appropriate equations, from simulations of the process,¹⁷ and also from experience with the analytical solution of the problem of chemical reaction zone.²⁴ We believe that the important features of the original problem are not lost after making the assumptions listed below.

- (1) The experimental setup can be described by one-dimensional reaction-diffusion equations (the gel is in a test tube whose length is much larger than its diameter).
- (2) The concentration of the outer electrolyte (a_0) is assumed to be much larger than that of the inner electrolyte (b_0) and it is also assumed that $a(0, t)$ is kept fixed at $x = 0$, [$a(0, t) = a_0$]. In experiments one typically has $0.005 \leq b_0/a_0 \leq 0.1$.
- (3) Reaction zones and the precipitation bands are much narrower than the diffusion length.
- (4) All concentration profiles can be approximated by straight lines in the neighborhood of the reaction zones and precipitation bands.
- (5) The slopes of the straight lines are determined by the diffusion lengths and by the asymptotic concentrations of the reacting species.

- (6) An existing precipitation band acts as a sink [with $b(x_n, t > t_n) = 0$ or $c(x_n, t > t_n) = 0$ boundary condition] for the inner electrolyte and for the intermediate compound (this is an assumption about the reaction and aggregation rates being sufficiently large).

Using the above assumptions, we can derive relatively simple expressions for $p(a_0, b_0)$ for all three classes of theories (in Sec. II for supersaturation of ion-product, in Sec. III for nucleation and droplet growth, and in Sec. IV for induced sol-coagulation theories). The results are compared both with the corresponding numerical solutions of the nonsimplified models and with experimental data. Section V contains our final remarks.

In closing the Introduction, we list the symbols frequently used in the text:

- $a(x, t)$ - concentration of outer electrolyte, A ;
- $b(x, t)$ - concentration of inner electrolyte, B ;
- a_0, b_0 - initial concentrations of A and B ;
- $\kappa = b_0/a_0$ - dimensionless ratio of initial concentrations;
- $c(x, t)$ - concentration of sol (or intermediate compound);
- D_a, D_b, D_c - diffusion coefficients of $A, B,$ and C ;
- D_f - effective diffusion coefficient of reaction front ($A + B \rightarrow C$);
- q^* - ion-product threshold;
- c^* - nucleation (coagulation) threshold;
- a^* - threshold for induced coagulation;
- x_n - position of the n -th precipitation band;
- t_n - time of formation of the n -th band;
- $1 + p = x_{n+1}/x_n$ - spacing coefficient.

II. ION-PRODUCT SUPERSATURATION

Let us begin with the simplest case of the reaction $A + B \rightarrow D$. The ion-product supersaturation theory¹⁰⁻¹³ is based on the assumption that precipitation of D at time t and at a site x occurs if the product of ion concentrations $a(x, t)b(x, t)$ exceeds a threshold value

$$a(x, t)b(x, t) \geq q^*. \tag{4}$$

In the mean-field theory, the equations describing this reaction-diffusion process are given by

$$\frac{\partial a}{\partial t} = D_a \frac{\partial^2 a}{\partial x^2} - k\theta(ab - q^*) - \lambda abd, \tag{5}$$

$$\frac{\partial b}{\partial t} = D_b \frac{\partial^2 b}{\partial x^2} - k\theta(ab - q^*) - \lambda abd, \tag{6}$$

$$\frac{\partial d}{\partial t} = k\theta(ab - q^*) + \lambda abd, \tag{7}$$

where D_a and D_b are the diffusion constants of A and B , and $\theta(x)$ is the step function describing an infinitely sharp threshold for precipitation with k being the rate constant. The last terms on the right-hand sides represent the aggregation onto the existing precipitate of concentration $d(x, t)$. The initial conditions to the above equations are given by $a(x, 0) = a_0\theta(-x)$, $b(x, 0) = b_0\theta(x)$, and $d(x, 0) = 0$.

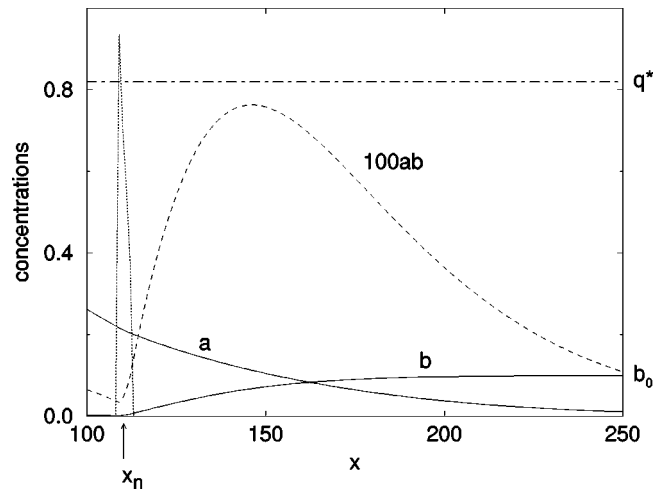


FIG. 1. Concentration profiles in the ion-product supersaturation model of Liesegang phenomena. Concentrations are measured in units of a_0 while the unit of length is $\sqrt{D_a/ka_0}$. The ion-product, ab , and its critical value, q^* , are measured in units of a_0^2 and they are magnified by a factor 100 for better visibility.

These equations can be solved numerically, and our analytical expression found for $p(a_0, b_0)$ in the above process is in accord with the numerical results. Before deriving the results, however, let us show how the structure of the result may emerge from a simple dimensional analysis.

If we assume that both the precipitation (k) and aggregation (λ) rates go to infinity, then it follows from dimensional considerations that the dimensionless spacing coefficient can be expressed through the available dimensionless combinations of the parameters, and so we have

$$p = P \left(\frac{b_0}{a_0}; \frac{D_b}{D_a}; \frac{q^*}{a_0 b_0} \right). \tag{8}$$

Further simplification can be made by assuming that P is not singular in its first argument and by setting this argument to zero since in experiments $b_0/a_0 \ll 1$. Then the Matalon-Packter law can emerge only if P is linear in its third argument, thus giving

$$p = P_1 \left(\frac{D_b}{D_a} \right) + P_2 \left(\frac{D_b}{D_a} \right) \frac{q^*}{a_0 b_0}. \tag{9}$$

We emphasize that this is not a derivation of the desired result. This is, however, what we shall show to be valid in the experimentally investigated range ($0.05 < p < 0.4$) of possible p -s. Our calculation is based on a simple analytical approach combined with numerical evaluation of P_1 and P_2 .

Figure 1 gives a characteristic picture showing the concentration profiles as well as the ion-product profile past the formation of the precipitation band x_n and just before the appearance of the $(n + 1)$ -th band. It is clear from the figure that the linearization of the concentration profiles is a good assumption, and, accordingly, in the neighborhood of x_n , we can approximate the concentrations as

$$a(x, t) = a_0 \left(1 - \frac{x}{\sqrt{2D_a t}} \right), \tag{10}$$

$$b(x,t) = \frac{b_0}{\sqrt{2D_b(t-t_n)}}(x-x_n). \quad (11)$$

The condition for the $n+1$ -st band to appear is that the maximum of the ab product reaches the value q^* . This leads to the following two equations:

$$a(x_{n+1}, t_{n+1})b(x_{n+1}, t_{n+1}) = q^*, \quad (12)$$

$$\frac{\partial}{\partial x}[a(x,t)b(x,t)]_{x_{n+1}, t_{n+1}} = 0. \quad (13)$$

The second equation gives a simple relationship between t_{n+1} , x_n and x_{n+1} ,

$$\sqrt{2D_a t_{n+1}} = 2x_{n+1} - x_n, \quad (14)$$

which allows us to eliminate t_{n+1} from Eq. (12) and to obtain an equation for x_{n+1}/x_n and x_n/x_{n-1} .

Assuming now that n is large enough that we can use the approximation

$$\frac{x_{n+1}}{x_n} \approx \frac{x_n}{x_{n-1}} = 1+p, \quad (15)$$

and one obtains the following equation for p ,

$$\Phi(p) = \frac{p^{3/2}(1+p)}{(1+2p)^2 \sqrt{2+p}} = \sqrt{\frac{D_b}{D_a}} \frac{q^*}{a_0 b_0}. \quad (16)$$

This equation clearly has a $p > 0$ solution for small values of $\zeta \equiv \sqrt{D_b/D_a} q^*/(a_0 b_0)$. p increases with ζ and goes to infinity for $\zeta \rightarrow 1/4$, accounting for the fact that no bands can be formed if $a_0 b_0$ is too small for ab to reach the critical value q^* .

At first sight, the Matalon-Packter law does not follow from this theory, since p depends on a_0 and b_0 only through $a_0 b_0$. Furthermore, another problem is that, for small p , we obtain Wagner's result,¹¹ namely the dependence of p on a_0 is of the form

$$p \sim a_0^{-2/3}, \quad (17)$$

in contrast to the Matalon-Packter prediction $p \sim 1/a_0$. However, one should notice that the range of p where $p \sim a_0^{-2/3}$ holds is certainly much smaller than the experimentally observed values $0.05 < p < 0.4$. In this latter interval, $\Phi(p)$ is very well approximated as a straight line (see Fig. 2) with parameters $\Phi(p) = -0.0035 + 0.2p$. Thus, to a good approximation, we can write (16) as a Matalon-Packter law with $F(b_0) = 0.02$ and $G(b_0) \sim 1/b_0$,

$$p = 0.02 + 5 \sqrt{\frac{D_b}{D_a}} \frac{q^*}{a_0 b_0}. \quad (18)$$

In this approach we obtain $P_1 = \text{const.}$ and $P_2 \approx \sqrt{D_b/D_a}$. Numerical solution of Eqs. (5) and (6) indicates that, in reality, the p is given to an excellent accuracy by

$$p \approx 0.18 - 0.052 \left(\frac{D_b}{D_a}\right)^{1/3} + \left[7.5 - 2.57 \left(\frac{D_b}{D_a}\right)^{1/6}\right] \frac{q^*}{a_0 b_0}. \quad (19)$$

For $D_a = D_b$, the order of magnitude for $F(b_0) \sim 0.12$ agrees with the order of magnitude values of F in

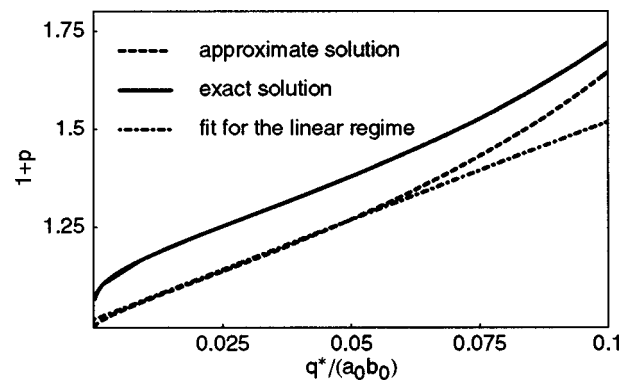


FIG. 2. Dependence of spacing coefficient $1+p$ on $q^*/(a_0 b_0)$ as given by the ion-product supersaturation theory for $D_a = D_b = 1$. The full line corresponds to the solution of Eqs. (5) and (6), the dashed line to our approximate theory. The dot-dashed line shows the linear dependence for small $q^*/(a_0 b_0)$.

experiments⁶ and the $1/a_0$ dependence is also the experimentally observed behavior. However, in experiments, $F(b_0)$ is not a universal number. It changes not only as D_b/D_a is varied, but it also depends on b_0 .⁶ Furthermore, the experimentally observed $G(b_0)$ is also more varied than being just $G(b_0) \sim 1/b_0$. Thus we must conclude that although it is possible to derive the Matalon-Packter law from the ion-product supersaturation theory, the resulting functions $F(b_0) \sim \text{const}$ and $G(b_0) \sim 1/b_0$ are too simple to account for experimental observations.

III. NUCLEATION AND GROWTH

The theory at the next level of complexity assumes that the $A+B$ reaction yields the precipitate D through an intermediate compound C . This compound may, in principle, be a molecule AB but it may as well be a sol particle formed by A and B and, possibly, by some other background ions. All of this rather complicated situation is described by assuming that the C -s can be treated as diffusing species which precipitate if their concentration exceeds a threshold c^* . The precipitate, D , grows by collecting the neighboring C -s and the various theories differ in the sophistication of the description of this nucleation and growth process.^{16,17} In our case the nucleation threshold is sharp at c^* and precipitate will be assumed to be a perfect sink for the C -s.

In order to understand the formation of precipitate, we observe that the reaction zone (where the C -s are produced) is narrow²⁴ and that $c(x,t)$ reaches its maximum there (see Fig. 3 for characteristic concentration profiles just before the $n+1$ -st band forms). The n -th band acts as a sink and thus the C -s (or about half of them) formed at the front, x_f , end up in this band.

With a good approximation, we can assume that at time t_{n+1} , when c reaches the threshold value c^* and the $(n+1)$ -th band is about to form, the concentration of C -s exhibits a triangular shape and it varies linearly between $c(x_n) = 0$ and $c(x_{n+1}) = c^*$. As a consequence, we can estimate the current flowing to the n -th band as

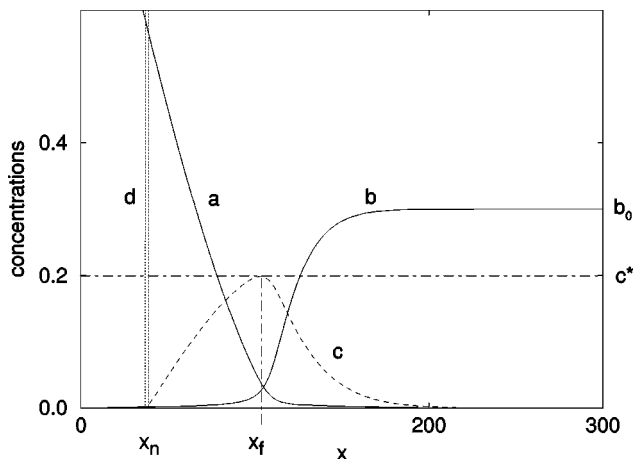


FIG. 3. Concentration profiles in the nucleation and growth model of Lie-segang phenomena. Units are the same as in Fig. 1.

$$|j| = D_c \frac{c^*}{x_{n+1} - x_n} \tag{20}$$

Next we note that the front becomes quasistationary in the large-time limit (its velocity goes as $\dot{x}_f \sim 1/\sqrt{t}$) and so we can assume that the above expression for the current is valid in the whole time interval $[t_n, t_{n+1}]$ (numerical solutions of the reaction-diffusion equations support this assumption). Then the amount of C which disappears into the n -th band during the time interval $[t_n, t_{n+1}]$ can be computed as

$$N_C \approx |j|(t_{n+1} - t_n) = D_c c^* \frac{t_{n+1} - t_n}{x_{n+1} - x_n} \tag{21}$$

On the other hand, N_C can also be estimated as the amount of C -s produced by the front $[c_0(x_{n+1} - x_n)$, where c_0 is a constant²⁴] minus the C -s which are in the triangle shape, $c^*(x_{n+1} - x_n)$,

$$N_C \approx (c_0 - c^*) \cdot (x_{n+1} - x_n) \tag{22}$$

Equating the two estimates of N_C then yields

$$\frac{D_c c^*}{c_0 - c^*} = \frac{(x_{n+1} - x_n)^2}{t_{n+1} - t_n} \tag{23}$$

We can use now the fact that the band is formed at the front whose position, x_f , is determined by an effective diffusion coefficient D_f ,²⁴

$$x_{n+1} \equiv x_f(t_{n+1}) = \sqrt{2D_f t_{n+1}}, \tag{24}$$

and find

$$\frac{p}{1+p/2} \approx p = \frac{D_c c^*}{D_f (c_0 - c^*)} \tag{25}$$

The parameters D_c and c^* in the above expression are material parameters. The dependence of p on a_0 and b_0 enters through the effective diffusion coefficient D_f of the front and through the concentration, c_0 , of C -s left behind by the moving front. The remaining task is thus to determine D_f and c_0 . We start with the case of $D_a = D_b$, which can be discussed with relative ease.²⁴ It has been shown for this case that D_f/D_a is determined from the following equation:

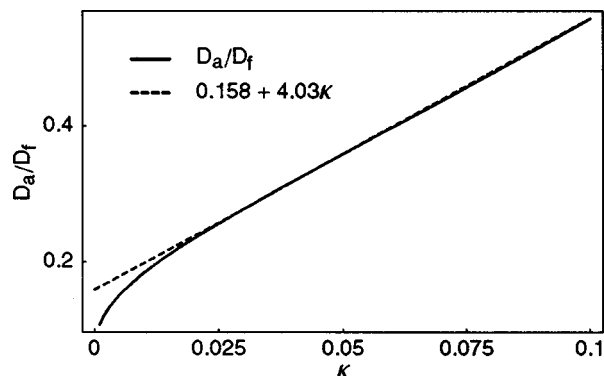


FIG. 4. Inverse of the effective diffusion constant of the front D_f as a function of $\kappa = b_0/a_0$, for $D_a = D_b = 1$.

$$\text{erf}\left(\frac{D_f}{2D_a}\right) = \frac{1 - \kappa}{1 + \kappa}, \tag{26}$$

where $\text{erf}(x)$ is the error function²⁶ and $\kappa = b_0/a_0$. The remarkable feature of the solution of this equation is that, for the experimentally relevant values $0.005 \leq \kappa \leq 0.1$, the inverse of D_f is very well approximated by a linear function of κ (see Fig. 4),

$$\frac{D_a}{D_f} \approx \eta_1 + \eta_2 \cdot \kappa \approx 0.158 + 4.03 \cdot \kappa \tag{27}$$

This is an important observation since it follows from (25) that $p \sim 1/D_f$ for small p and the Matalon-Packter law will emerge as a consequence of the above equation.

The general case $D_a \neq D_b$ is more complicated but the results are similar. The effective diffusion coefficient, D_f , is obtained from solution of the following equation,²⁵

$$H\left(-\sqrt{\frac{1}{2} \frac{D_f}{D_a}}\right) = \frac{a_0}{b_0} \sqrt{\frac{D_f}{D_a}} H\left(\sqrt{\frac{D_a}{2D_b} \frac{D_f}{D_a}}\right), \tag{28}$$

where $H(x) \equiv [1 - \text{erf}(x)] \exp(x^2)$. The behavior of D_a/D_f as a function of κ for $D_b \neq D_a$ is similar to that seen in Fig. 4. One can observe that D_a/D_f is linear in κ in the experimentally relevant region and thus Eq. (27) emerges again but the constants η_1 and η_2 are now dependent on D_b/D_a .

We turn now to the calculation of c_0 . The starting point is the observation that the width of the reaction zone is much smaller than the diffusion length²⁴ and thus the reaction zone can be approximated as a point at $x_f(t) = \sqrt{2D_f t}$ where both concentrations a and b approach zero. This means that the field $b(x, t)$ satisfies the diffusion equation with the reaction term replaced by the boundary condition $b(x = x_f, t) = 0$ and the other boundary condition being $b(x \rightarrow \infty, t) = b_0$. Once this moving boundary problem is solved, the number of C -s, N_C , produced up to a given time is obtained by the time integral of the current $|j_b| = D_b \partial b / \partial x$ evaluated at x_f . Finally, c_0 is found by dividing N_C by the advance of the front in time t , $c_0 = N_C/x_f$ (here we use the fact that the density of C -s produced by the front is constant in space²⁴). The result of this calculation is given by

$$c_0 = \frac{b_0}{\sqrt{\pi}} \sqrt{\frac{2D_b}{D_f}} \exp\left(-\frac{D_f}{2D_b}\right) \left[1 - \operatorname{erf}\left(\sqrt{\frac{D_f}{2D_b}}\right)\right]^{-1}. \quad (29)$$

For $D_a = D_b$ and $\kappa \ll 1$ we can use Eq. (26) in conjunction with the asymptotics of the error function²⁶ to obtain $c_0 = b_0$. The physical meaning of this result is clear. For $\kappa \ll 1$, we have $D_b \ll D_f$ and thus the front moves fast into the region of B -s and, consequently, the B -s can be treated as immobile particles yielding $c_0 = b_0$. Corrections to the $c_0 = b_0$ result can also be calculated using again the asymptotics of the error function.²⁶ To first order in D_b/D_f , we find

$$c_0 \approx b_0 \left(1 + \frac{D_b}{D_f}\right) = b_0 \left(1 + \frac{D_b}{D_a} \frac{D_a}{D_f}\right). \quad (30)$$

We can use now the linearity of D_a/D_f in $\kappa = b_0/a_0$ to obtain the following parametrization for c_0 :

$$c_0 = b_0(\sigma_1 + \sigma_2 \kappa), \quad (31)$$

where $\sigma_1 = 1 + \eta_1 D_b/D_a$ and $\sigma_2 = \eta_2 D_b/D_a$ are numbers of the order of 1. Since σ_1 and σ_2 are of the same order of magnitude and since $\kappa \ll 1$, in the following we shall neglect the κ term in (31),

$$c_0 \approx \sigma_1 b_0. \quad (32)$$

It is important to note here that a similar omission of the b_0/a_0 term would not be justified in the linearized form of D_a/D_f .²⁷ There we have a constant term, $\eta_1 \approx 0.2$, that is an order of magnitude smaller than the coefficient, $\eta_2 \approx 4$, in front of b_0/a_0 . Thus, for the relevant values of b_0/a_0 , the two terms contribute equally.

The expressions (30), (31), and (32) remain good approximations up to the point where $D_b/D_f \approx 1$. This happens, however, only at rather large values of D_b/D_a for $\kappa \ll 1$. Since the diffusion coefficients of usual electrolytes in aqueous solutions are usually within a factor 2 of each other²⁷ and their ratios rarely exceed 5,²⁸ we believe that the approximation (31) can be used for realistic experimental setups.

Having determined D_f and c_0 , we can now return to Eq. (25) for p and find again a version of the Matalon-Packter law,

$$p = \frac{D_c c^* \eta_1}{D_a(\sigma_1 b_0 - c^*)} + \frac{D_c c^* \eta_2 b_0}{D_a(\sigma_1 b_0 - c^*) a_0} = F(b_0) + \frac{G(b_0)}{a_0}. \quad (33)$$

In order to gain confidence in the above result, we have calculated p for κ in the experimental range $0.005 < \kappa < 0.1$ by using the appropriate reaction-diffusion equations [Eqs. (5), (6), and (7) must be modified and supplemented by another equation in order to take into account the nucleation and growth processes described at the start of the section (for details see Ref. 17)]. The results are displayed in Fig. 5 where the Matalon-Packter law derived above (solid line on the figure) is shown to perform very well considering the simplicity of the derivation. It should be noted that nonlinear

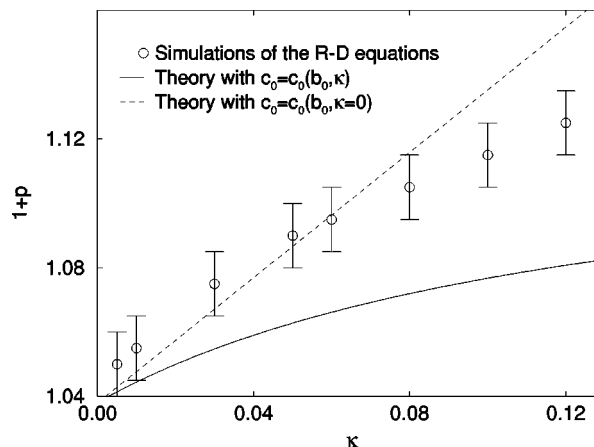


FIG. 5. Spacing coefficient for the nucleation and growth theory. The $\kappa = b_0/a_0$ dependence of p is shown for the following choice of parameters: $D_b/D_a = 1$, $D_c/D_a = 0.2$, $c^*/b_0 = 0.633$, and with all the reaction rates taken to be large. The dashed line is the ‘linear’ Matalon-Packter law (33) while the solid line is the ‘nonlinear’ version of (33) where the κ -dependence of c_0 (31) is kept.

dependence on κ sets in for $\kappa \geq 0.06$ and that taking into account the κ -dependence of c_0 (dashed line) modifies the straight line with the right curvature.

One can observe from Eq. (33) that the nucleation and growth theory gives more complicated b_0 dependences for $F(b_0)$ and $G(b_0)$ than the ion-production theory. Power law forms for F and G are found in the limit of $c^* \ll b_0$ (which might be the experimental limit) where one obtains $F(b_0) \sim 1/b_0$ and $G(b_0) \sim \text{constant}$. It is remarkable that these are similar to the ion-product results but with the roles of F and G interchanged. Comparing the two theories, we see that the nucleation and growth theory performs better in the sense that it can produce power law behavior for $F(b_0)$ as observed in some experiments and, at the same time, has a $G(b_0)$ which depends on b_0 more weakly but it is a decreasing function of b_0 in agreement with experiments.

In conclusion, the nucleation and growth theory provides us with a Matalon-Packter law that is closer to experiments and, perhaps, describes some of them. Nevertheless, the functions F and G appear to be too rigid to accommodate all experimental findings. It should also be noted that this theory has a prediction $G(b_0)/F(b_0) \sim b_0$ that is experimentally easily distinguishable from the prediction of the ion-product theory, $G(b_0)/F(b_0) \sim 1/b_0$.

IV. INDUCED SOL-COAGULATION

The induced sol-coagulation theory^{14,15} is a generalization of the nucleation and growth theory. The sol, C , is produced at the reaction front in the $A + B \rightarrow C$ reaction and it flocculates if the following two conditions are satisfied. First, c must exceed a supersaturation threshold c^* and, second, the concentration of the outer electrolyte, a , must be above the critical coagulation concentration threshold, a^* . The second condition arises in systems where the A ions screen the repulsive electrostatic interaction among the sol particles.

Figure 6 shows characteristic concentration profiles in this process just as the $n + 1$ -st band is appearing. The first

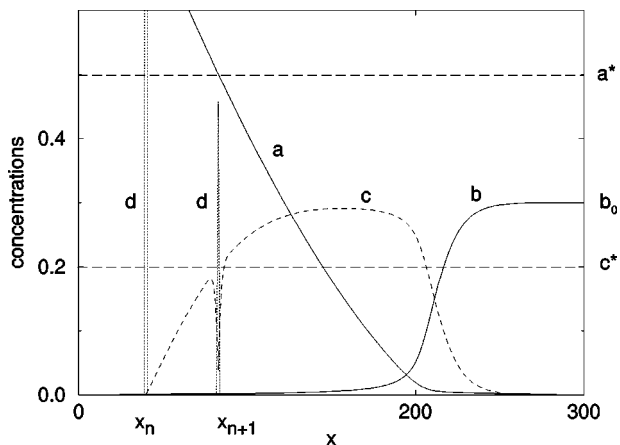


FIG. 6. Concentration profiles and thresholds in the induced sol-coagulation theory. Units are the same as in Fig. 1.

remarkable feature of this picture is that the reaction front is way ahead of the precipitation zone (this does seem to happen in some experiments¹⁹). This is understandable, since $a(x_f, t) \rightarrow 0$ at the front, while at the place where precipitation occurs one must have $a(x_{n+1}, t_{n+1}) \geq a^*$. The second important feature is that the reaction front leaves C -s behind at a fixed concentration c_0 , as already discussed in the previous section. In order that precipitation could occur, the parameters must be assumed such that $c_0 > c^*$. Further assuming that the sol does not diffuse too fast ($D_c \ll D_a$), one of the conditions for precipitation ($c \geq c^*$) is always satisfied behind the front and far away from the last existing band (x_n).

Consequently, the position, x_{n+1} , where the next band appears will be determined by the arrival of the concentration “front” $a = a^*$ to a position where $c = c^*$. Since the a and c profiles near x_n can be written as $a = a_0(1 - x/x_f)$ and $c = c_0(x - x_n) / \sqrt{2D_c(t - t_n)}$, the above conditions yield

$$\frac{c_0(x_{n+1} - x_n)}{\sqrt{2D_c(t_{n+1} - t_n)}} = c^*, \tag{34}$$

$$a_0 \left(1 - \frac{x_{n+1}}{x_f(t_{n+1})} \right) = a^*, \tag{35}$$

where $x_f(t) = \sqrt{2D_f t}$ is the position of the reaction front at time t .

In order to calculate p , we note now that Eq. (35) yields

$$\frac{x_{n+1}}{x_f(t_{n+1})} = 1 - \frac{a^*}{a_0} = \frac{x_n}{x_f(t_n)}. \tag{36}$$

The above equation can then be used in conjunction with $x_f(t_{n+1}) = \sqrt{2D_f t_{n+1}}$ to obtain p from Eq. (34),

$$\frac{p}{1 + p/2} \approx p = \frac{2D_c c^{*2}}{D_f c_0^2 (1 - a^*/a_0)^2}. \tag{37}$$

Since the values of D_f and c_0 come from reaction $A + B \rightarrow C$ which is decoupled from the next stages of nucleation and growth processes, the calculations and approximations of these quantities can be taken over from Sec. III. Moreover, we shall assume that a^* is much smaller than a_0 so

that the right-hand side of Eq. (37) can be expanded in a^*/a_0 . There is no experimental information on a^* and, although $a^*/a_0 \ll 1$ seems to be a natural assumption, we must be cautious with the $a^*/a_0 \rightarrow 0$ limit. The problem is that the picture we are working with for the induced sol-coagulation theory (Fig. 6) is not valid for arbitrary small a^* . Indeed, the fact that the position of the $A + B \rightarrow C$ reaction front, x_f , is far ahead of the point of formation of the $n + 1$ -st band means that diffusion length of the C particles is smaller than $x_f(t_{n+1}) - x_{n+1}$,

$$\sqrt{2D_c(x_{n+1} - x_n)} < x_f(t_{n+1}) - x_{n+1}. \tag{38}$$

Using Eqs. (36) and (37) and neglecting higher order terms in p and a^*/a_0 , the above equation yields

$$\frac{D_c c^* a_0}{D_f c_0 a^*} < \frac{1}{2}. \tag{39}$$

The meaning of this result is the following. The place where the new band nucleates moves to the $A + B \rightarrow C$ reaction zone and thus the inequality (38) gets violated upon increasing D_c or c_* and decreasing a^* . It is clear thus that, at fixed values of the other parameters, a^*/a_0 cannot be taken to zero.

The lack of the limit $a^*/a_0 \rightarrow 0$ has the consequence that the result for the nucleation and growth theory (33) cannot be obtained from (37). The matter of finding an expression for p valid in the $a^*/a_0 \rightarrow 0$ limit and reducing to (33) appears to be a rather difficult task since various length scales become comparable approaching this limit. We have not been able to obtain such an interpolating formula.

Returning to (39), we see that the material parameters can be such (e.g., if $c^*/c_0 \ll 1$) that a^*/a_0 can be small without the inequality (39) being violated. For such a range of parameters we can expand (37) in a^*/a_0 and obtain again a version of the Matalon-Packter law,

$$p = \frac{2D_c c^{*2}}{D_a \sigma_1^2} \frac{\eta_1}{b_0^2} + \frac{2D_c c^{*2}}{D_a \sigma_1^2} \cdot \frac{(2\eta_1 a^* + \eta_2 b_0)}{b_0^2 a_0}. \tag{40}$$

The spacing coefficient (40) can again be compared with that obtained from the appropriate reaction diffusion equations (the equations for the nucleation and growth theory must be augmented with the condition that nucleation can occur only if $a > a^*$). An exhaustive numerical study is practically impossible due to the number of parameters in the problem ($\kappa, a^*/a_0, c^*/a_0, D_b/D_a, D_c/D_a$), plus the rates of reaction, nucleation, and aggregation. One can easily miss regimes of nontrivial behavior in this high dimensional parameter space and we claim with this numerical study only that the Matalon-Packter law as given by Eq. (40) is indeed observed for a reasonable range of parameters (Fig. 7).

As one can see from (40), the induced sol-coagulation theory provides us with

$$F(b_0) \sim 1/b_0^2, \quad G(b_0) \sim (\alpha + \beta b_0)/b_0^2. \tag{41}$$

The power law form $F(b_0) \sim b_0^{-2}$ is close to what has been observed in some experiments⁶ and the fact that $G(b_0)$ is a decreasing function of b_0 is also in accord with the observations. It should also be clear that a more precise

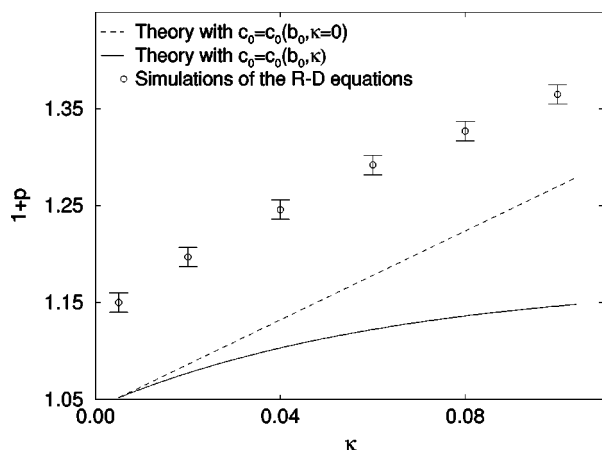


FIG. 7. Spacing coefficient for the induced sol-coagulation theory. The dependence of p on $\kappa = b_0/a_0$ is displayed for the following choice of parameters: $D_b/D_a = 1$, $D_c/D_a = 0.3$, $c^*/b_0 = 0.86$, $a^*/b_0 = 7.8$, and with all the reaction rates taken to be large. The dashed line is the ‘linear’ Matalon-Packter law (40) while the solid line is the ‘nonlinear’ version of (40) where the κ -dependence of c_0 (31) is kept when going from Eq. (37) to Eq. (40).

theory of the induced sol-coagulation process should reproduce, in the $a^*/a_0 \rightarrow 0$ limit, the result $F \sim b_0^{-1}$ obtained in the nucleation and growth theory. Thus, assuming that the crossover between the b_0^{-2} and the b_0^{-1} behaviors is smooth, one should be able to find regimes where $F(b_0) \sim b_0^\gamma$ with $1 \leq \gamma \leq 2$. Since this covers a large portion of the experimentally observed range $0.2 \leq \gamma \leq 2.7$, we conclude that the induced sol-coagulation theory provides the best description of the pattern formation in Liesegang phenomena.

V. FINAL REMARKS

Our main results are summarized in Eqs. (19), (33), and (40) giving the Matalon-Packter law for the three main theories, respectively. Comparing these formulas, we arrived at our main conclusion, namely that the induced sol-coagulation theory is the best in describing the experimental observations on the spacing coefficient of Liesegang patterns.

There is no doubt that the arguments used in the derivation of p can be refined and made more precise. The main aim of our work, however, was the demonstration that the Matalon-Packter law can be understood in terms of simple pictures for which it is possible to develop analytical arguments. We hope that one can build on these results and achieve a better understanding of Liesegang phenomena. In particular, it would be important to find a description of the induced sol-coagulation process which contained the crossover to results for the nucleation and growth model. Furthermore, we have just considered the simplest cases associated with the reaction $A + B \rightarrow C$. In experiments, equally important are the $A_2 + B \rightarrow C$ and $A + B_2 \rightarrow C$ cases and, obviously,

one should also explore the possibilities associated with these and, possibly, more complicated reaction schemes. Finally, an interesting and important test of the conclusion that the induced sol-coagulation theory is preferable in the studies of Liesegang phenomena would be the application of this theory for the *quantitative* description of revert patterns.^{18,29,30,31}

ACKNOWLEDGMENTS

We thank B. Chopard, P. Hantz, and T. Unger for useful discussions. This work has been partially supported by the Swiss National Science Foundation in the framework of the Cooperation in Science and Research with CEEC/NIS, by the Hungarian Academy of Sciences (Grant No. OTKA T 019451), and by the EPSRC, United Kingdom (Grant No. GR/L58088).

- ¹M. C. Cross and P. C. Hohenberg, *Rev. Mod. Phys.* **65**, 851 (1994).
- ²R. E. Liesegang, *Naturwiss. Wochenschr.* **11**, 353 (1896).
- ³H. K. Henisch, *Periodic precipitation* (Pergamon, New York, 1991).
- ⁴Harry W. Morse and G. W. Pierce, *Diffusion and Supersaturation in Gelatine*, Proceedings of the American Academy of Arts and Sciences, **38**, 625 (1903).
- ⁵K. Jablczynski, *Bull. Soc. Chim. Fr.* **33**, 1592 (1923).
- ⁶R. Matalon and A. Packter, *J. Colloid Sci.* **10**, 46 (1955).
- ⁷A. Packter, *Kolloid-Z.* **142**, 109 (1955).
- ⁸There are systems that display revert patterns, namely the distance between the bands decreases with band number instead of increasing as in the normal Liesegang phenomena. In these cases $x_n/x_{n-1} \rightarrow 1$, i.e., $p=0$ and the Matalon-Packter law is clearly not applicable.
- ⁹S. C. Müller, S. Kai, and J. Ross, *J. Phys. Chem.* **86**, 4078 (1982).
- ¹⁰W. Ostwald, *Lehrbuch der allgemeinen Chemie* (Engelman, Leipzig, 1897).
- ¹¹C. Wagner, *J. Colloid Sci.* **5**, 85 (1950).
- ¹²S. Prager, *J. Chem. Phys.* **25**, 279 (1956).
- ¹³Ya. B. Zeldovitch, G. I. Barrenblatt, and R. L. Salganik, *Sov. Phys. Dokl.* **6**, 869 (1962).
- ¹⁴N. R. Dhar and A. C. Chatterji, *Kolloid-Z.* **37**, 2 (1925); *J. Phys. Chem.* **28**, 41 (1924).
- ¹⁵S. Shinohara, *J. Phys. Soc. Jpn.* **29**, 1073 (1970).
- ¹⁶G. T. Dee, *Phys. Rev. Lett.* **57**, 275 (1986).
- ¹⁷B. Chopard, P. Luthi, and M. Droz, *Phys. Rev. Lett.* **72**, 1384 (1994); *J. Stat. Phys.* **76**, 661 (1994).
- ¹⁸M. Flicker and J. Ross, *J. Chem. Phys.* **60**, 3458 (1974).
- ¹⁹S. Kai, S. C. Müller, and J. Ross, *J. Chem. Phys.* **76**, 1392 (1982).
- ²⁰R. Feeney, S. L. Schmidt, P. Strickholm, J. Chadam, and P. Ortoleva, *J. Chem. Phys.* **78**, 1293 (1983).
- ²¹G. Venzl, *J. Chem. Phys.* **85**, 1996, 2006 (1986).
- ²²There is a class of theories (Refs. 18–21) which attributes the Liesegang band formation to the instability present in the postnucleation coarsening process. These theories, however, cannot explain the regular aspects of the band spacing.
- ²³D. A. Smith, *J. Chem. Phys.* **81**, 3102 (1984).
- ²⁴L. Gálfı and Z. Rác, *Phys. Rev. A* **38**, 3151 (1988).
- ²⁵Z. Koza, *J. Stat. Phys.* **85**, 179 (1996).
- ²⁶*Handbook of Mathematical Functions*, edited by M. Abramowitz and I. A. Stegun (Dover, New York, 1965).
- ²⁷J. Koryta, J. Dvorák, and L. Kavan, *Principles of Electrochemistry* (Wiley, New York, 1993).
- ²⁸B. Chopard, M. Droz, J. Magnin, Z. Rác, and M. Zrinyi (in preparation).
- ²⁹P. Mathur and S. Ghosh, *Kolloid-Z.* **159**, 143 (1957).
- ³⁰N. Kanniah, F. D. Gnanam, P. Ramasamy, and G. S. Laddha, *J. Colloid Interface Sci.* **80**, 369 (1980).
- ³¹P. Hantz, Master thesis, Eötvös University, Budapest, 1998.